Growth and Printability of Multilayer Phase Defects on EUV Mask Blanks

Ted Liang, Erdem Ultanir, Guojing Zhang, Seh-Jin Park
Intel Corporation, 2200 Mission College Blvd., Santa Clara, CA 94054
Erik Anderson, Eric Gullikson, Patrick Naulleau, Farhad Salmassi
Lawrence Berkeley National Laboratory, 1 Cyclotron Rd, Berkeley, CA
Paul Mirkarimi, Eberhard Spiller, Sherry Baker
Lawrence Livermore National Laboratory, Livermore, CA

ABSTRACT

The ability to fabricate defect-free mask blanks is a well-recognized challenge in enabling extreme ultraviolet lithography (EUVL) for semiconductor manufacturing. Both the specification and reduction of defects necessitate the understanding of their printability and how they are generated and grow during Mo-Si multilayer (ML) deposition. A ML phase defect can be depicted by its topographical profile on the surface as either a bump or pit, which is then characterized by height or depth and width. The complexity of such seemingly simple phase defects lies in the many ways they can be generated and the difficulties of measuring their physical shape/size and optical effects on printability. An effective way to study phase defects is to use a programmed defect mask (PDM) as 'model' test sample where the defects are produced with controlled growth on a ML blank and accurate placement in varying proximity to absorber patterns on the mask. This paper describes our recent study of ML phase defect printability with resist data from exposures of a ML PDM on the EUV micro-exposure tool (MET, 5X reduction with 0.3NA).

1. INTRODUCTION

Projection lithography using EUV light at 13.5nm is the preferred choice for post-193nm optical patterning for high volume manufacturing of semiconductor devices[1]. One of the top three challenges for EUVL is the ability to produce quality ML blanks with zero defects[2]. Two major factors contribute to the risk in ML blank production: extremely stringent defect requirements due to the use of short wavelength of 13.5nm light and the complex and delicate steps of blank making process. For example, any defect causing a mere 3.5nm difference in the reflective EUV optical path will result in a 180 degree phase shift. While the engineering of the Mo-Si ML structure is well established and blanks can be routinely produced with good peak reflectivity and uniformity, the feasibility has yet to be demonstrated for producing of producing blanks meeting anticipated defect specifications[3].

Mask defect specifications are ultimately determined by the yield impact to device performance which correlates to resist CD (critical dimension as measured mostly by a SEM) variations in a particular lithographic patterning layer. Such methodology of gauging resist CD change is commonly referred as *defect printability*. However, specification for defects on *ML blanks* is not a trivial endeavor because of the many factors we shall consider, including not only the impact to resist imaging of patterns on the mask, but also how the device patterns will be placed on the blank during e-beam writing. For example, a ML defect located between two narrow lines may cause the lines to bridge, while the same defect may cause no harm if it were under or far away from the line. Therefore, it is not unreasonable to expect that most device layouts may tolerate the existence of a small number of defects on the ML blank. A useful ML blank may not necessarily be 'defect-free'.

This paper describes our study of the growth and printability impact of ML defects in the following four sections. We first discuss the nature and growth of defects in a ML blank, followed by a description of the PDM with ML defects of surface heights ranging from <1nm to 8nm. Then, we present resist print data showing the defect printability at three different illumination conditions and the effect of defect proximity to absorber patterns. From these data, we propose ML defect specifications for dense and isolated line patterns. Finally, we discuss the factors we must take into account when defining ML defect requirements for a useful ML blank.

2. NATURE AND GROWTH OF ML DEFECTS

Defects in a ML blank may originate from two distinctive sources: imperfect substrates and the ML fabrication process. For the sake of a simplified discussion in this paper, we will only consider two types of defect morphologies – pits and bumps. Figure 1 is a schematic cross-sectional view of a patterned EUV mask highlighting the layer structures and types of bump defects. Both pits and bumps can cause disturbances to the ML which affect the phase and/or amplitude of the reflected EUV light. Such optical manifestation of pits and bumps depends on the ML deposition process. Three coating techniques are employed most for fabricating ML reflectors – e-beam evaporation, magnetron sputtering, and ion beam sputtering (IBD). IBD is preferred over e-beam and magnetron for mask blank fabrication due to its low level of defect generation mainly because of the highly collimated ion beams. Off-normal incidence is usually done in an IBD system to produce ML coatings with more uniform layer thickness (hence uniform EUV reflectivity) over the entire substrate. Under such conditions, defects on the substrate generally propagate through the ML stack by the so-called 'decorative effect' of ML coating, such that the topography of the ML surface carries a magnified signature of the underlying substrate defect[3 4].

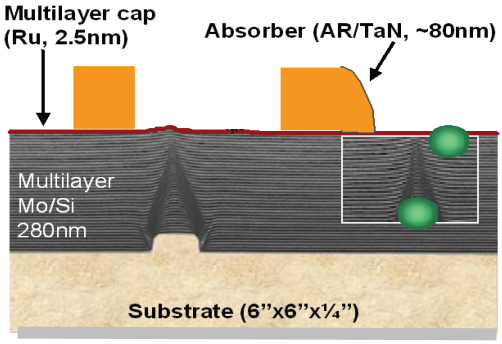

Figure 1: Schematic of photomask for EUV lithography. ML blank defects can be originated from substrate and added during ML deposition (shown as insert), with the former most likely to be phase defects.

Defect evolution in an IBD system has been investigated with both theoretical modeling and extensive experimentation[5 6 7]. By choosing the proper angle of deposition and etch back processing, both pits and particles on the substrate can be rendered to low or zero topography at the ML surface (such as the one shown in Figure 1). This so-called 'smoothing' process is a powerful technique in reducing the impact of substrate defects.

From the above discussions of ML deposition processes, one soon comes to the realization that a meaningful specification of substrate defects must specify the deposition process (i.e. normal, off-normal, smoothing) under which the ML blank is fabricated. On a finished blank, all we can measure are deviations from a flat and smooth surface. A typical state-of-the-art ML blank with Ru-capping has a surface roughness around 0.15nm rms in the high frequency range. Above such a 'noise' floor, we can measure a defect in terms of its

height (depth for pit) and width, usually as full-width-at-half-maximum (FWHM) assuming a Gaussian shape.

Previous ML defect discussions have been mostly based on simulation[8] with limited resist print data[9]. A widely acceptable defect specification needs extensive resist print data with well-defined test masks and realistic exposure conditions. Simulation models shall be calibrated with such printability data. The combined use of model and resist print can then provide better predictability of defect requirements for future pattern geometries. The following discussions will focus on ML bump defects.

3. DESIGN, FABRICATION AND CHARACTERIZATION OF TEST MASK

The effect of ML defects on pattern printing is studied with a PDM comprised of *Multilayer* defects placed near absorber *Patterns* (MP). Such *MP-PDM* includes absorber line and contact patterns of different CDs and pitches, a wide range of ML defect sizes and shapes, and varied proximity of ML defects to the adjacent absorber patterns. Figure 2 shows the overall MP-PDM design and layout. *The convention for describing the values in this paper is: all resist and mask CDs are referred to the dimensions at the wafer level (1X) and all defect sizes are measured on the mask level (5X).*

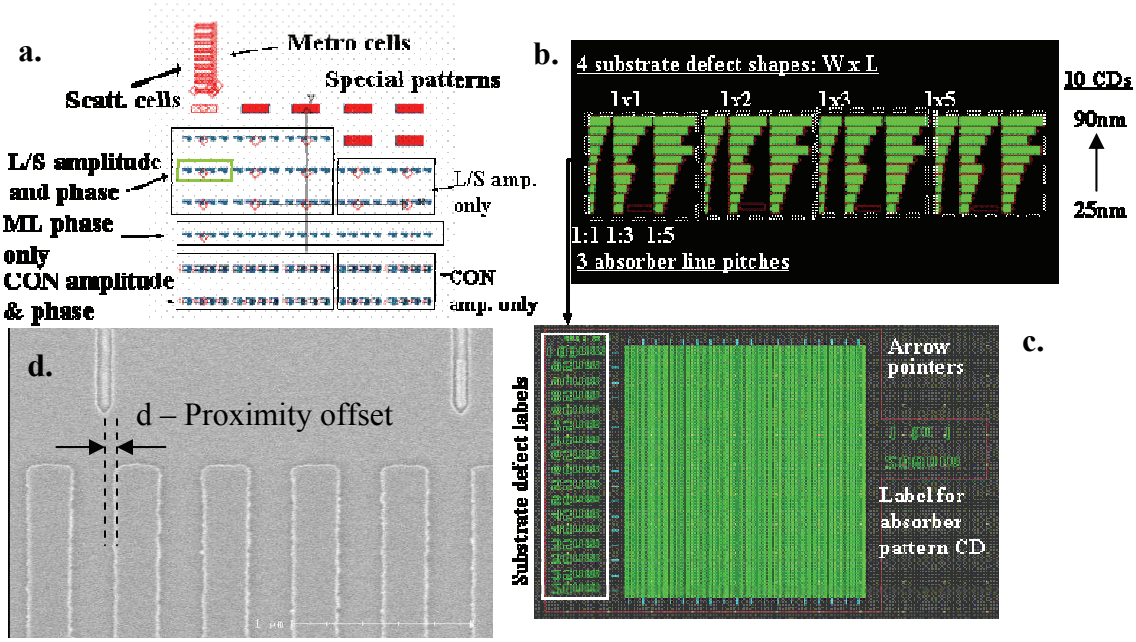

Figure 2: Description of MP-PDM. a) Layout includes various fields in 5x7 arrays; b) One field showing 4 cells of different ML defect shapes; c) A sub-cell of square ML defects of 17 sizes (inside the box) under 40nm 1:1 absorber lines; d) SEM image of 1:1 lines with arrows pointing to ML defect.

The exposure fields on the mask are partitioned into groups of different types of patterns and structures (Figure 2a). One field layout is shown in an expanded view in Figure 2b) which consists of four cells of identical absorber line:space (L:S) patterns labeled as 1x1, 1x2, 1x3 and 1x5, indicating four shapes (width x length) of the ML defects under each cell. For each cell, there are three sub-cells containing three L:S ratios (1:1, 1:3, 1:5). In each sub-cell, there are 10 line CDs in the vertical direction starting with 25nm from the bottom to 90nm at the top. Under every set of absorber lines with the same CD, there are 17 sizes of ML defects placed in systematically varying proximity to the absorber lines. A detailed view of the 40nm

1:1 L:S and associated ML defects is displayed in Figure 2d. The labels on the left side mark the 17 sizes, from 20nm to 100nm in 5nm steps. The exact location of each ML defect with respect to its adjacent absorber line is at the intersection formed by the vertical and horizontal arrows. The proximity of ML defect to respective lines is varied in 50nm steps on the mask. Each defect of the same size and location was repeated 3 times on the mask and the results described later are the average over these three measurements. Figure 2d) is an SEM image showing one site on the mask, with offset *d* as the proximity of a ML defect to the line edge.

The MP-PDM fabrication involves many steps. First, we patterned special alignment marks on the substrate for accurately registering both the programmed ML defects and absorber patterns. Then programmed patterns on super-smooth quartz substrates were formed with a 48nm thick HSQ (hydrogen Silsesquioxane) resist layer after e-beam lithography. The HSQ pattern has 17 sizes from 20nm to 100nm in 5nm steps (thus the labels in Figure 3d) in four shapes (1x1 square, 1x2, 1x3 and 1x5 rectangles as indicated in Figure 2b). Our ML coating process in an IBD tool was carefully tuned for smoothing performance, as previously discussed in section 2, to produce the desired range of ML bump sizes from these seeded HSQ patterns on the substrate. The HSQ size will be used to label corresponding ML defects. After ML coating, the programmed ML defects were measured with AFM.

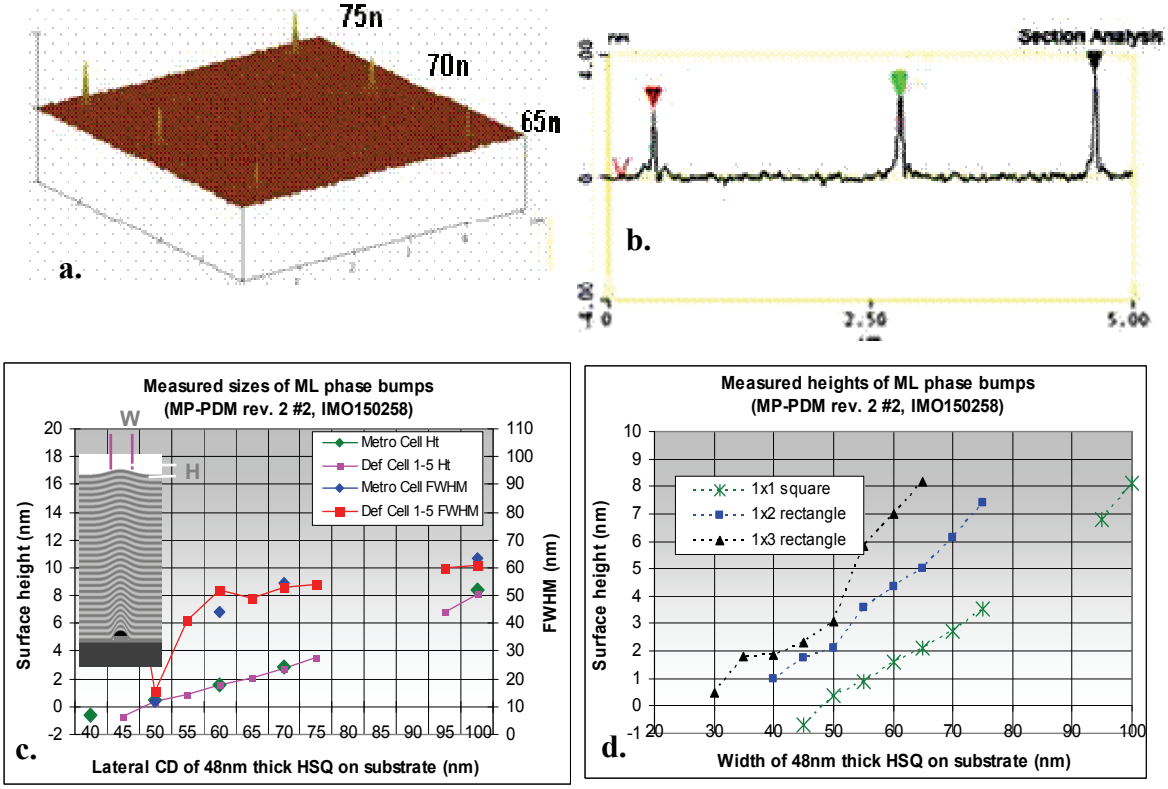

Figure 3: Sizes and shape of ML bumps corresponding to the HSQ patterns on substrates. a and b shows 3D image and line scan of three defect sizes as labeled.

Plotted in Figure 3 are the sizes of ML bumps as a function of the lateral dimension of the HSQ patterns on the substrate from which the ML bumps were grown. Plot 3c shows that the surface height is in the range of ~0 to 8nm and the FWHM is around 40nm to 60nm for square HSQ originated ML defects. Note that the ML coating process completely smoothed out any substrate HSQ square patterns below 50nm. We estimate that all these ML bumps are phase

defects. As expected, ML defects from elongated HSQ patterns (1x2, 1x3 and 1x5) are much larger as produced with the same coating process.

After ML coating, TaN absorber with anti-reflective layer (75nm total thickness) was deposited at Intel's EUV mask Pilotline and patterned at LBNL using the KRS e-beam resist process. The ML defect sizes as well as the proximity distance between ML defects and absorber lines were further confirmed and measured with AFM on the completed MP-PDM. The absorber line CDs were measured with standard CD-SEM.

4. RESIST PRINTS FROM MP-PDM

The MP-PDM was exposed on both EUV micro-exposure tools – one at Intel with a Xe discharge produced plasma source and one at the ALS with synchrotron radiation source, with the latter being more flexible in providing different illumination conditions. The MET is a small field (400μ x 600μ, 1X) EUV stepper with a NA of 0.3 and 5X reduction. The incidence angle of EUV light onto the mask is 3.6°. The flare for the MET optics is about 5-7%[10]. Three types of illuminations were used (Figure 4) to investigate their effect on ML phase defect printability. There is a central obscuration of radius $\sigma = 0.3$ for all illuminations. The resist used in the exposure on the MET at ALS is Rohm and Haas MET-1K with a sensitivity of about 20mJ/cm^2 at 112nm thickness for printing dense lines about 40nm to 60nm. Current resist performance limits the printing to >40nm 1:1 lines without mask bias or over dose. The line edge roughness (LER) is about 4-5nm, setting a lower measurement limit for CD changes. Details of the process window have been previously reported elsewhere[11, 12]. Due to page limits for this article, we will only present resist print data from square ML defects (i.e., 1x1 sub-cell in Fig. 2) for 1:1 absorber lines.

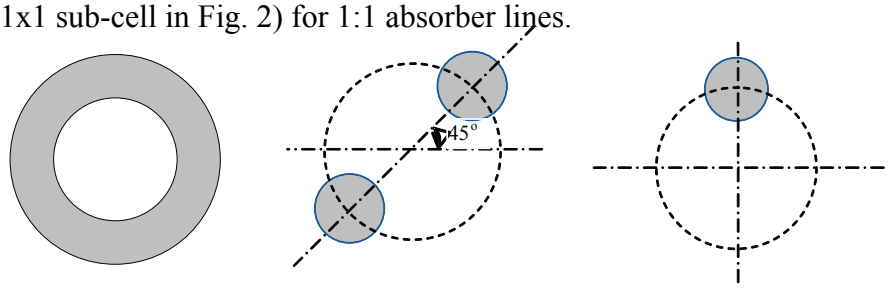

Figure 4: MET illuminations used in this printability study.

Resist CDs were measured from CD-SEM images using offline software[13]. Instead of using values from a single line to measure CDs at the defect site, we extracted the CDs from averaging over a length of about 15nm (~λ/4NA) to increase accuracy (see two horizontal lines in Figure 5a). The resist CD change caused by defects was measured either for the space or a single line depending on whether two lines or only one line was affected by the defect.

Typical SEM images showing resist lines printed at best dose and focus from the defect cells on the MP-PDM are displayed in Figure 5 for the 50nm and 40nm 1:1 absorber lines where 3 sets of ML defects (labeled on the left side by each SEM image) were located at the center between two lines. As designed, each set contains 3 identical defects and indeed they showed the same effect on printed resist lines.

Effect of illumination: We studied the effect of different illuminations on defect printability using 50nm 1:1 lines. The resist was exposed with annular, Y-monopole, and 45° dipole illuminations on the same defect cell on the MP-PDM. Shown in Figure 6 are resist

images for the same 3 sets of defects: 75nm, 80nm and 85nm. From the SEM images one can see the obvious difference - ML defects are most printable with dipole illumination while annular and Y-monopole illumination exhibit similar effects. This is possibly due to the higher resolution in y-direction under dipole illumination such that defects are better resolved. Plotted in figure 6 are also the space CD changes (%ΔCD/CD) as function of more defect sizes, again indicating worst printability under dipole conditions.

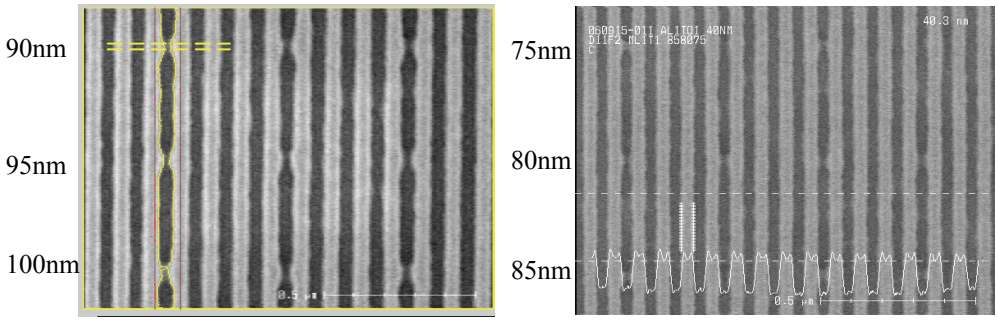

a: 50nm 1:1 b: 40nm 1:1

Figure 5: Example of ML defects centered between two 40nm and 50nm 1:1 lines printed with Y-monopole illumination. The labels on the right sides indicate the HSQ sizes.

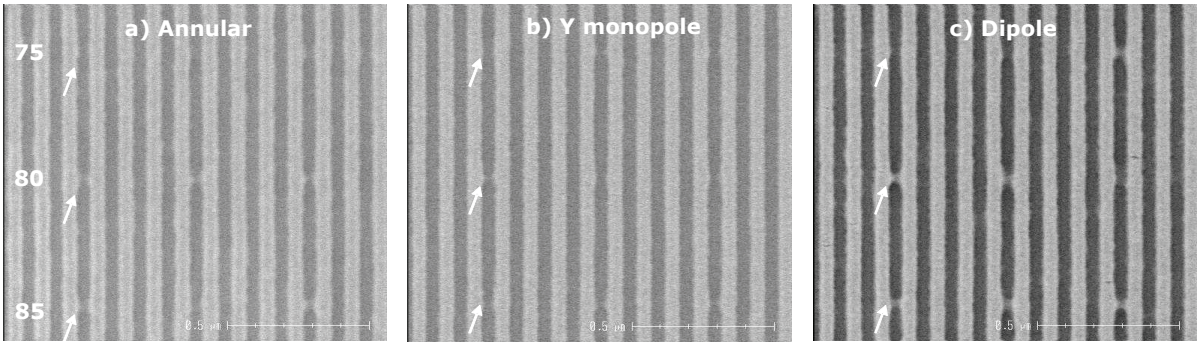

Figure 6: Effects of illumination on printability using 50nm 1:1 lines as example. The defects are at center between two lines.

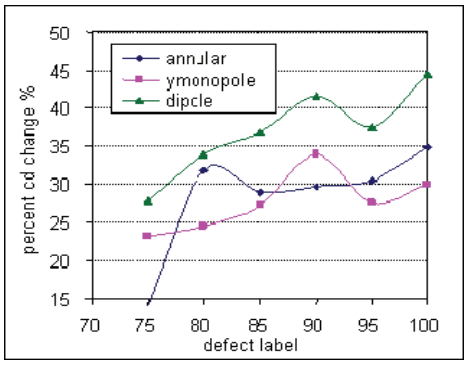

Effect of defect proximity*:* Resist CD changes as a function of ML defect proximity to absorber lines printed under three illuminations are plotted in Figure 7. Every curve in the graph represents a set of ML defects of different sizes at the same proximity to the absorber lines. As defined by *d* in Figure 2, offset zero indicates the center of the ML defect is at the edge of the absorber line (i.e., absorber covers half of the defect). We can draw the following general conclusions from these data. 1) defect printability is sensitive to illumination condition for all proximities; 2) printability is worse for dense lines when the defect is at the center between two lines; 3) ML phase defects can effectively be rendered non-printable by covering it with absorber, hence the benefit of optimized placement of device patterns on 'defective' ML blanks.

Effect of defocus: Similar to 193nm PSM, printability of ML phase defects is expected to vary with depth of focus. As an example, plotted in Figure 8 is space CD change for 45 nm 1:1 lines as a function of size of ML defects printed at focus and +100nm defocus with

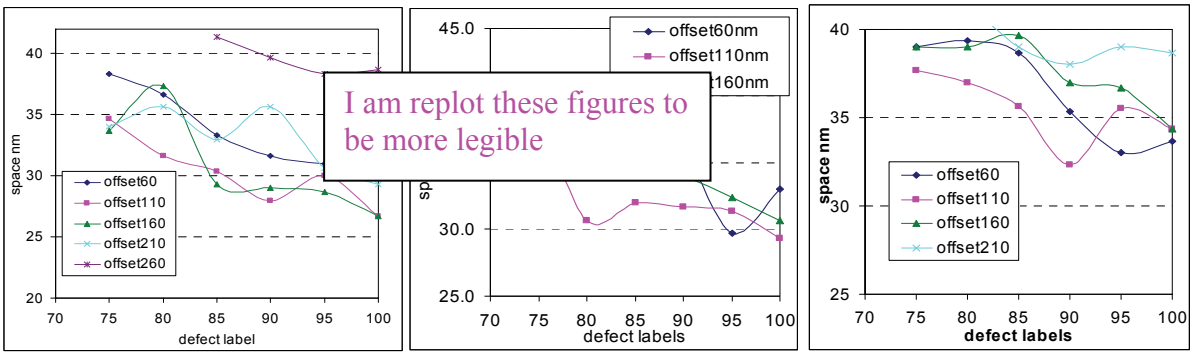

a. Dipole **b. Annular** **c. Y-mono**

Figure 7: Printability sensitivity to defect proximity to the absorber lines using 50nm 1:1 lines as example. Different curves represent different proximity offsets in step of 50nm (5x).

Y-monopole). Printability increases with defocusing. We observed reduced focus effect for defects with greater heights, which may indicate that larger ML defects contain amplitude components.

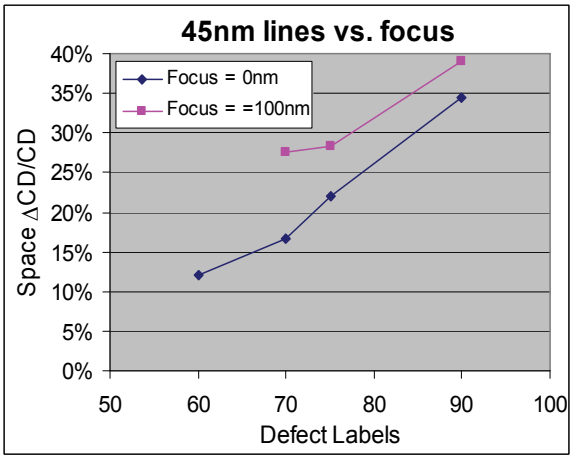

Figure 8: Focus effect on ML defect printability.

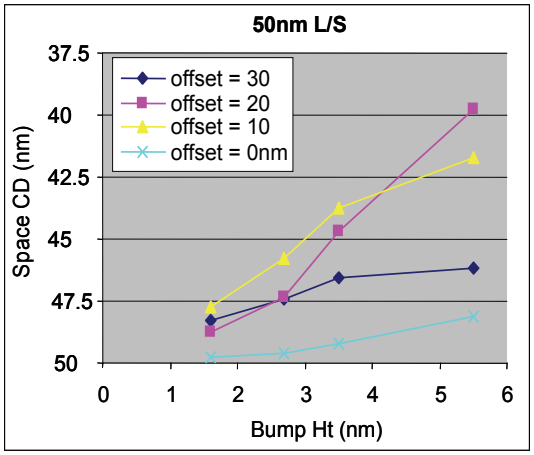

Figure 9: SSA simulation results for Y-monopole.

One of our main goals for collecting resist print data is to make comparisons with and validate simulation models. Some preliminary simulation results are shown in Figure 9 for 4 defect sizes at varying proximity to 50nm 1:1 lines. There are mismatches between experimental resist print data and modeling results. Work is ongoing towards understanding the possible contributing factors, including resist effects, accuracy of AFM data in representing actual ML phase defect size and shape, and possibly 3D effects[14]. Our results show that the aerial image intensity from ML phase bumps is very sensitive to the FWHM of defects with same height. AFM is very accurate for measuring bump height, but not as good for measuring width due to tip effects. TEM imaging of cross sections of ML bumps will be done to confirm the exact defect profile.

5. DISCUSSION OF ML DEFECT SPECIFICATION

The likely design for a pre-production EUV full-field exposure tool (PPT) uses a uniform scan field and the property of such illumination is similar to the annular fill in the MET. By scaling to a 4X, 0.25NA PPT-like printing from MET printability data, we can estimate the maximum size of allowable ML defects for patterning dense and isolated lines. The scaled defect size for printing on a PPT is $D_{PPT} = D_{MET}$ (4/5*0.3/0.25) $=0.96*D_{MET} \approx D_{MET}$

assuming similar resist performance and ML defect behavior. The printability plot obtained from the MET with annular illumination, as shown in Figure 7b, can essentially directly represent printing using q PPT. For example, if no more than 20% ΔCD/CD is allowed in printing 50nm 1:1 lines, the spec for ML bump defects in the worst case scenario (when defect is at center of space) is about 3nm height x 55nm FWHM (corresponding to a 75nmx75nm defect of 48nm thick on the substrate with ML smoothing process). The spec for printing isolated lines is larger than this value.

The importance of defect specification is to ensure device performance as well as to guide defect reduction in blank fabrication and the development of inspection and metrology tools. In manufacturing, defect specifications must consider inspection tool capability, particularly substrate inspection. For example, ML deposition with near normal incidence in an IBD tool will produce a 3nm ML bump from a 30nm particle defect on substrate. However, with off-normal incidence currently used for ML deposition, a 3nm ML bump could be produced from a much smaller substrate particle[4]. Either a ML smoothing process[7] or deposition with an optimized incident angle can be beneficial in alleviating the need for extremely high quality substrates.

6. SUMMARY

We have presented our experimental study of the growth and printability of ML phase defects. The size and shape of ML bumps originating from substrate defects strongly depends on deposition conditions. We used a specially tuned coating process to produce programmed ML defects of varying size and shape and place them near absorber patterns. Resist printing was done on MET tools under annular, dipole and monopole illuminations. Printability of ML phase bumps clearly depends on illumination conditions, with dipole producing the worst effect. For patterning dense lines, the worst case location for a ML defect is at the middle of two lines. A ML phase bump with a height of 3nm at the surface causes 20% CD change for 50nm 1:1 lines.

7. ACKNOWLEDGEMENTS

We appreciate the expert support for MET exposures from Paul Denham, Brain Hoef, Gideon Jones, Jerrin Chui, and Ken Goldberg from LBNL and Jeanette Roberts from Intel. Discussions with Prof. Andrew Neureuther are always stimulating and insightful.

8. REFERENCES

[1] See for example, P.J.Silverman, *J. Microlith. Microfab. Microsyst.* 4, 5 (2005).

[2] Source, resist and mask blank have been the top three risk areas for enabling EUVL surveyed by Sematech.

[3] R.V. Randive, A. Ma, P.A. Kearney, D. Krick, I. Reiss, P.B. Mirkarimi and E. Spilller, J. Microlith. Microfab. Microsysr. 5(2) (2006).

[4] P.B. Mirkarimi and D.G. Stearns, *Appl. Phys. Lett., Vol. 77(14), 2243 (2000).*

[5] D.G.Stearns, P.B.Mirkarimi, and E.Spiller , *Thin Solid Films* 446, 37 (2004).

[6] P.B.Mirkarimi, E.Spiller , S.L.Bak er, J.C.Robinson, D.G. Stearns, J.A.Liddle, F.Salmassi, T.Liang, and A.R.Sti vers, *Microelec. Eng.* 77, 369 (2005).

[7] P. B. Mirkarimi, E. Spiller, S. L. Baker, D. G. Stearns, J. C. Robinson, D. L. Olynick, F. Salmassi, J. A. Liddle, T. Liang, and A. R. Stivers, *J. Nanosci. Nanotechnol.,* Vol.6, 28 (2006)

[8] E.M. Gullikson; E. Tejnil, T. Liang, A.R. Stivers; *Proc. SPIE, Vol. 5374, 791(2004).*

[9] Y. Tezuka, J. Cullins, Y. Tanaka, T. Hashimoto, I. Nishiyama and T. Shoki, Proc. SPIE. Vol. 6517 (2007).

[10] P. Naulleau, et al, *J. Vac. Sci. Technol*. B23(6), 2840 (2005).

[11] P. Naulleau, C. Rammeloo, J. Cain, K. Dean, P. Denham, K. Goldberg, B. Hoef, B. La Fontaine, A. Pawloski, C. Larson and G. Wallraff, *Proc. SPIE*, Vol. 6151 (2006).

[12] T. Liang, G. Zhang, P. Naulleau, A. Myers, S. Park, A. Stivers and G. Vandentop, *Proc. SPIE*, Vol. 6283 (2006)

[13] SUMMIToffline analysis software from EUV Technology.

[14] C.H. Clifford and A.R. Neureuther, Proc. SPIE, Vol. 6517 (2007).